PROCEEDINGS OF SPIE

SPIEDigitalLibrary.org/conference-proceedings-of-spie

Cryogenic germanium detectors for a weakly interactive massive particle (WIMP) dark-matter search

Walter Stockwell, D. Akerib, E. Aubourg, P. D. Barnes, A. Cummings, et al.

Walter Stockwell, D. Akerib, E. Aubourg, P. D. Barnes, A. Cummings, Angela Da Silva, J. Emes, Sunil Golwala, Eugene E. Haller, S. Margulies, B. Pritychenko, R. R. Ross, Bernard Sadoulet, T. Shutt, Garth Smith, J. Taylor, S. White, B. A. Young, "Cryogenic germanium detectors for a weakly interactive massive particle (WIMP) dark-matter search," Proc. SPIE 2280, EUV, X-Ray, and Gamma-Ray Instrumentation for Astronomy V, (16 September 1994); doi: 10.1117/12.186825

SPIE.

Event: SPIE's 1994 International Symposium on Optics, Imaging, and Instrumentation, 1994, San Diego, CA, United States

Cryogenic germanium detectors for a WIMP dark matter search

W. Stockwell[a], D. Akerib[a], É. Aubourg[a], P. D. Barnes Jr.[a], A. Cummings[a], A. Da Silva[d], J. Emes[c], S. Golwala[a], E. E. Haller[b,c], S. Margulies[a], B. Pritychenko[a,e], R. R. Ross[a,c], B. Sadoulet[a], T. Shutt[a], G. Smith[c], J. Taylor[c], S. White[a], B. A. Young[a]

Center for Particle Astrophysics; and
[a]Department of Physics, [b]Department of Material Science and Mineral Engineering,
University of California at Berkeley, Berkeley, CA 94720;
[c]Lawrence Berkeley Laboratory, 1 Cyclotron Rd., Berkeley, CA 94720;
[d]Department of Physics, University of British Columbia, 6224 Agricultural Rd.,
Vancouver, BC V6T 1Z1, Canada
[e]Baksan Neutrino Observatory, Institute for Nuclear Research, Russian Academy of Science, Moscow, Russia

ABSTRACT

We are preparing an experimental search for weakly interacting massive particle (WIMP) dark matter using cryogenic germanium detectors. These detectors measure both the ionization and phonons produced by particle interactions in the substrate. The ionization measurement uses low drift fields, ≈1 V/cm. The phonon measurement is made using neutron transmutation doped (NTD) germanium thermistors. Simultaneous detection of phonons and ionization allows us to discriminate between electron-recoil and nuclear-recoil events which gives a powerful method for isolating possible WIMP events (nuclear recoils) from background gamma ray events (electron recoils). Recent work on our understanding and optimization of these detectors will be presented.

1. INTRODUCTION

1.1 Dark Matter

One of the outstanding problems in cosmology today concerns the structure of the universe. A convenient measure of the geometry of the universe is the parameter Ω, the ratio of the mass-energy density of the universe, ρ, to the critical mass-energy density, ρ_c, needed for a flat universe. Astronomers can measure the amount of luminous matter seen in galaxies; this amount Ω_{lum} is typically 0.01, much less than 1.[1] However, by measuring the primordial abundances of the light elements, one can infer that the mass density in baryons, Ω_{bar}, is in the range 0.08 - 0.015, greater than the amount of luminous matter seen. This would seem to indicate that there must exist baryonic matter that does not glow. Recent attempts to detect baryonic dark matter in the halo of the Milky Way by gravitational microlensing of distant stars have reported a few events each.[2-4]

One can use the luminous matter in a galaxy as test particles to measure the gravitational potential in the galaxy. Assuming that the galaxy is thermalized, one can use the measured rotation curve and the virial theorem to measure the mass distribution in the galaxy. The mass density one obtains is much greater than Ω_{lum}, and is nearly too large to be compatible with the maximum mass density allowed in baryons from primordial nuclear synthesis. On larger distance scales, one can use clusters of galaxies in the same way, and find even larger measurements of Ω. Dynamical measurements over the largest distance scales, 100 Mpc, using velocity flows of clusters of galaxies have reported values of Ω in the range 0.2 - 1. Finally, one can make direct cosmological measurements of the curvature of the universe -- i.e., by doing number counts of galaxies vs. redshift. These experiments find values of Ω close to one. Also there is strong theoretical bias to have $\Omega = 1$, as it is hard to have a universe today with Ω close, but not equal, to 1 without fine tuning Ω at early times. Also

---

The CfPA cryogenic dark matter search is being done in collaboration with groups at U. C. Santa Barbara and Stanford University.

0-8194-1604-5/94/$6.00

inflationary models of the universe necessarily force $\Omega = 1$. All of the experimental determinations of Ω are difficult measurements and have correspondingly large errors, but they all point to a value of Ω significantly greater than that allowed in baryons. This indicates that there must be a non-baryonic element to the dark matter.

One generic solution to the problem of non-baryonic dark matter is a hypothetical particle that was in thermal equilibrium with the early universe, and whose relic abundance supplies the necessary energy density to close the universe. If the particles are non-relativistic when they freeze out, and they supply the mass necessary to make $\Omega=1$, they must have annihilation and scattering cross sections of order the weak scale, 10^{-38} cm^2, and will have a mass in the range from 10 GeV to 10 TeV.[5] These hypothetical particles are known as Weakly Interacting Massive Particles, or WIMPs. Note that these particles are a natural part of any supersymetric extension to the Standard Model.

1.2 A Cryogenic WIMP Detector

Assuming a Maxwellian velocity distribution for gravitationally bound WIMPs in the galactic halo, we can estimate the mean velocity of the dark matter flux on our detector as the solar system rotates through the dark halo. From this we can then estimate the mean energy deposition, as a function of WIMP mass, of an interaction in our detector. For a 10 GeV WIMP, the mean energy deposition is 0.5 keV. We can also calculate the event rate expected in our Ge detectors as a function of WIMP mass. Assuming an interaction cross section on the order of the weak scale, we expect an event rate of $\approx$0.4 events/keV/kg/day.

WIMPs are expected to preferentially deposit energy in the detector by scattering off of nuclei, whereas photons, which constitute most of the signal background, interact primarily with the electrons in the detector. Because electron recoils and nuclear recoils have different ionization efficiencies, the two types of events, in principle, can be distinguished. We have developed novel cryogenic particle detectors capable of directly measuring the ionization efficiency of particle events occurring in the detector substrate. We do this by simultaneously measuring the phonons and ionization produced by an event. For electron recoils, $\approx$33% of the initial energy goes into the production of electron-hole pairs. For nuclear recoils, the amount of energy appearing in ionization is even less, as little as 10%. Thus the ratio of the ionization and the phonon signal pulse heights provides important nuclear vs. electron recoil discrimination information. This discrimination allows us to veto the dominant source of background events in our detector, photons.

Both the low expected event rate and the relatively small event energies make WIMP dark matter search experiments quite challenging. Massive detectors with low energy thresholds and high energy resolution are required. In addition, the experiment must be performed in a low background environment, and implementation of an intrinsic background rejection scheme, such as ours based on the ionization efficiencies of nuclear and electronic recoils, is perhaps essential.

2. THE PHONON MEASUREMENT

Our detectors consist of high purity germanium disks onto which Neutron Transmutation Doped (NTD) germanium thermistors are attached. NTD germanium is made by exposing high purity germanium to neutrons from a nuclear reactor. The neutrons are absorbed by germanium atoms which are then unstable; the resulting decay products act as dopants in the germanium. The NTD method provides a homogenous and reproducible dopant concentration. The thermistors are attached either using a small amount of silver epoxy or using a gold-germanium eutectic bond. We bias the thermistors with a voltage across a large resistor, typically 10 - 40 MΩ. We operate the thermistors at a resistance $\approx$ 10 times lower than the bias resistor, so that the bias current is approximately set by the bias resistor. The detector is mounted on the mixing chamber of a dilution refrigerator and cooled to $\approx$ 20 mK. The voltage across the thermistor is measured with an FET mounted on the 4 K cold plate of the dilution refrigerator and connected to a room temperature low noise voltage amplifier.[7]

2.1 The Hot Electron Model

We currently understand our thermistors in terms of the Hot Electron Model. As shown by N. Wang, *et al.*[8], the behavior of our thermistors at an operating temperature of 20 mK is not consistent with an electric field effect model. At these low temperatures the electrons in the thermistor thermally decouple from the phonons in the thermistor. In the model, as shown pictorially in Figure 1, the electrons have a temperature, T_e, a heat capacity, C_e, and some conductance to the phonon system. The phonon system (we assume the phonons in the thermistor are well coupled to the phonons in the detector substrate) also has some temperature, T_ϕ, heat capacity, C_ϕ, and conductances to both the electron system and the heat sink. The electrical resistance of the thermistor is assumed to be a function only of the electron temperature, T_e. The resistance of the thermistor is well described by the parameterization

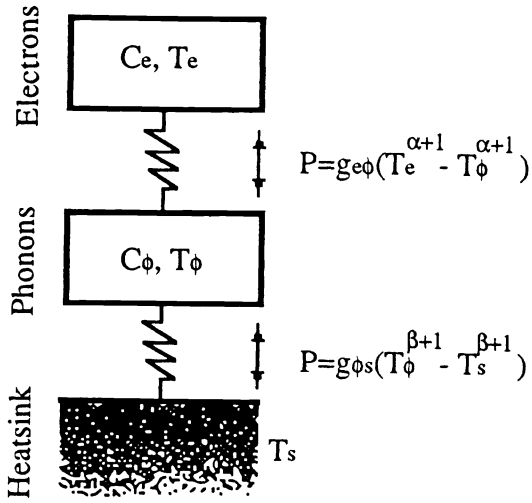

Figure 1. Schematic diagram of the hot electron model. The phonons in the thermistor and the detector crystal are assumed to be well coupled.

$$R(T_e) = \frac{A}{L}\rho_0 \exp\left(\sqrt{\Delta / T_e}\right), \tag{1}$$

where ρ_0 and Δ are parameters to be fit, A and L are the area and thickness of the thermistor, respectively, and T_e is the temperature of the electrons in the system. Typical values for our thermistors (NTD 29) are $\rho_0 \approx 0.1$ Ω-cm and $\Delta \approx 7$ K. The I-V curves of the thermistors are highly non-linear. Using this model, the I-V curve and the expected pulse height response of the thermistor to energy deposited in the detector can be predicted. The electron heat capacity and electron-phonon decoupling can be measured dynamically, by fitting pulses or by fitting the transfer functions of the thermistors at different bias voltages.

2.2 Thermistor Optimization

We built two devices, P1a and P1b, to better understand what parameters most greatly affect thermistor performance. Figure 2 is a diagram of these devices. Both P1a and P1b have four NTD thermistors mounted on a 2 cm diameter by 1 cm thick single crystal disk of high purity Ge. The thermistors on P1a were all the same geometry, 1.72 mm^2 x 0.88 mm thick, and were similarly mounted, but were of different NTD Ge types (NTD 28, NTD 29, NTD 12, and NTD 23). Different NTD types correspond to different initial neutron doses and thus different dopant concentrations. The thermistors on P1b were all of NTD 29, but were very different geometries (2.23 mm^2 x 0.31 mm, 3.53 mm^2 x 2.85 mm, 4.35 mm^2 x 0.49 mm, and 8.50 mm^2 x 1.17 mm). In addition, both P1a and P1b were operated with different amounts of heatsinking. Both sides of the detector crystal were boron implanted for ionization collection contacts. Both crystals had small gold pads (2.5 mm x 0.5 mm) deposited in the center of the top surface to use as a heater contacts. The resistance between the pads was ≈ 100 Ω; by electrically pulsing the pads, we could inject a known amount of heat into the crystal.

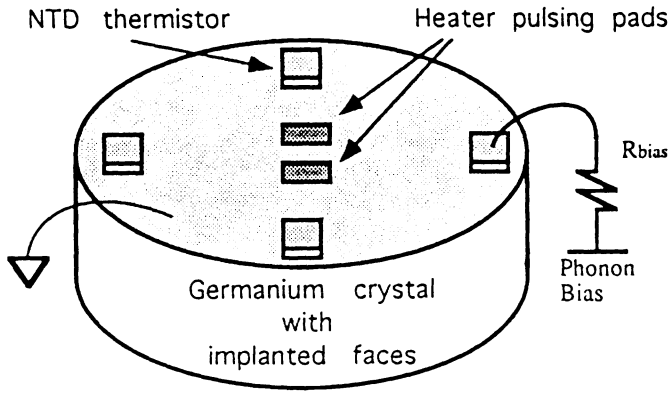

Figure 2. Diagram of the P series devices. Heatsinking was done through the tops of the thermistors or through the top of the crystal to the detector holder.

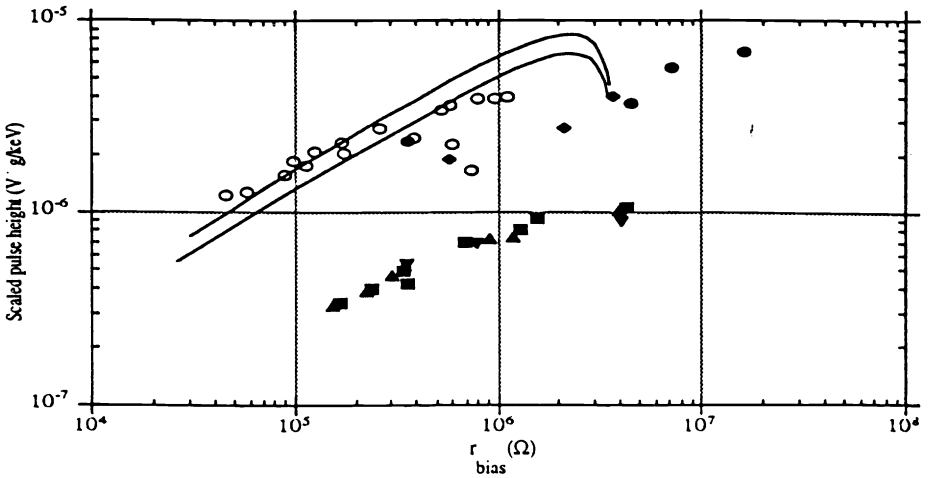

Figure 3. A comparison of the hot electron model and data from P1a, P1b, P2, and E4 for NTD 29 thermistors. The pulse height maxima are scaled by the mass of the detector substrate and the heater pulse energy. The lines show the calculated scaled pulse height vs. rbias for sensor 3 on P1a; the open symbols are the data.

The electron heat capacity, C_e, and the electron-phonon decoupling parameter, $g_{e\phi}$, were measured for each thermistor on P1a and P1b. In addition, the crystal-heatsink decoupling, $g_{\phi s}$, was measured for each configuration of the heatsinking.[9] The maximum pulse height vs. bias for each thermistor was measured for a given heater energy deposition. By scaling pulse height by the energy deposition and the mass of the crystal on which the thermistor is mounted, the performance of thermistors attached to different devices can be compared. (Figure 3) We found that for any thermistor on any device, in a given run, the pulse height maxima fall on a line proportional to $r_{bias}^{1/2}$ (r_{bias} is the resistance of the thermistor at the bias point). The scaling of the pulse height maxima like $r_{bias}^{1/2}$ is also seen in the hot electron model. The signal-to-noise ratio of the thermistors is the ratio of the pulse height to the noise in the measurement. Typically the noise in our measurements is dominated by the Johnson noise of the thermistor. Because both the pulse height and the Johnson noise of the thermistor scale like $r_{bias}^{1/2}$, the sensitivity of a thermistor is constant along this line. We have good qualitative agreement between these measurements and our hot electron model calculations.

The largest identifiable lever for affecting the sensitivity of the phonon measurement is changing the coupling between the crystal and the heatsink. For a given device, less heatsinking leads to a larger pulse height at a given r_{bias}. This is also seen in our model. Less heatsinking has the disadvantage of creating longer pulses, which typically have fall times from 10 ms to 100 ms depending on the exact heatsinking configuration.

2.3 Gold-germanium eutectic bond

We built a third test device, P2, to test the phonon transmission of the eutectic bonds between the Ge crystal and the NTD thermistors. The Ge crystal was the same size as those used for P1a and P1b. Four NTD 29 thermistors were attached, all 2.0 x 2.0 x 0.5 mm, the same size as one of the sensors on P1b. The sensors were attached using a eutectic method developed by W. Knowlton, et al., at Lawrence Berkeley Laboratories.[10] A gold film is deposited on both the Ge crystal and the NTD Ge thermistor to be attached. The thermistor is then pressed against the corresponding gold pad on the crystal, the whole assembly is heated above the Au-Ge eutectic temperature of 361 °C, and then slowly cooled. Small test pieces of Ge were bonded to test this method. The bonded pieces were cut across the joint, and the bond was examined with high resolution transmission electron microscopy. It was found that the Ge lattice was continuous across parts of the bond. For P2, two thermistors were attached using a 300 Å eutectic, one thermistor with a 500 Å eutectic, and one thermistor with a 1000 Å eutectic. (The "thickness" of the eutectic refers to the thickness of the gold film that is deposited onto both the crystal and the thermistor.) One of the 300 Å eutectic thermistors had its crystal axis deliberately misaligned by 8° from the crystal axis of the Ge crystal.

One interesting result was that all three of the sensors tested (the wiring on the 1000 Å eutectic thermistor circuit opened during cool down) had very similar electrical properties. Typically, thermistors mounted on devices show some scatter in their electrical and thermal properties, especially if mounted using silver epoxy. The thermistors had very similar I-V

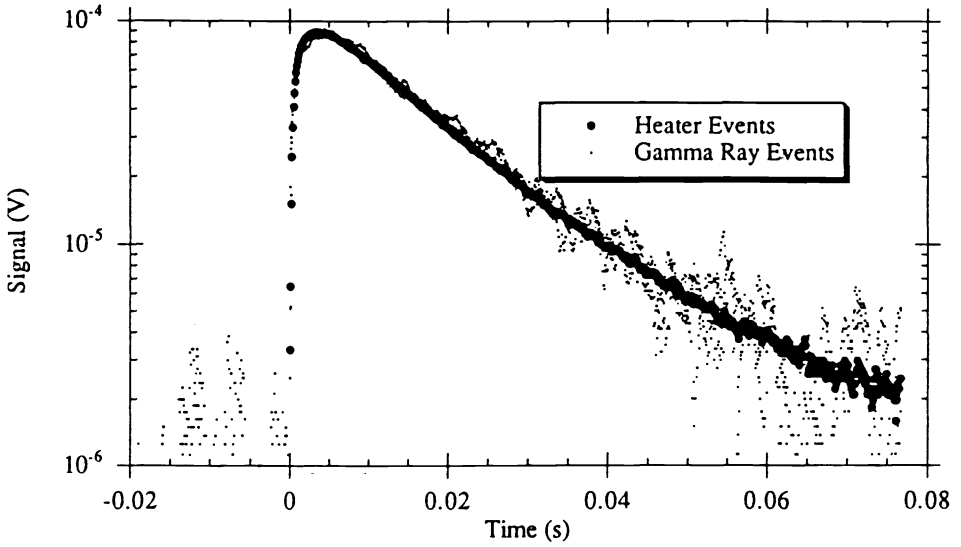

Figure 4. A comparison of pulses from heater events and gamma ray events in P2. These pulses were measured with the 300Å eutectic, aligned sensor.

characteristics, and the two sensors that were aligned with the crystal axis gave almost identical pulse height vs. bias. Measurements of $R(T_e)$ showed Δ varied by 3% from the average value of 7.03 K for the three thermistors; ρ_0 varied by 20% from the average value of 0.0975 Ω-cm. Variations in ρ_0 and Δ among otherwise identical NTD thermistors is usually attributed to stress and makes thermistor design somewhat unpredictable. We have found that eutectic bonds are a more reliable and predictable method than silver epoxy for mounting NTD thermistors .

Heat pulses of 1.56 MeV were injected through the heater pads and measured. Gamma ray events of comparable energy to the heater events were measured. This was done by defining a window in pulse height around the value we measured for the heater events. The gamma rays are presumably from compton scatters of background sources in the room such as ^{40}K. Figure 4 shows an average of 20 heater pulses and a few gamma pulses of comparable energy as measured with the 300 Å eutectic, aligned sensor. For each sensor, the pulse shapes are not significantly different between the heater events and the gamma ray events .

It is believed that a photon event should initially produce a "hot spot", with phonons on the order of the Debye temperature, 374 K in Ge.[11, 12] The initial phonons propagate away from the interaction site, and quickly decay into lower energy phonons. The lower energy phonons will travel ballistically to the surface of the detector, and will have temperatures on the order of 10 K.[13] In contrast, if we consider the implanted contacts as a metal with a low carrier density, the phonons produced by the heater events should be described by the hot electron effect in metals. We have not made this calculation, however if the electron heating is not severe, the phonons from the heater events should be nearly thermal. (As a worst-case estimate, if the electron-phonon decoupling in the contact is of comparable magnitude to that of the NTD Ge, the heater pulses would have heated the electrons in the contact to ≈50 mK.) The thin eutectic interface is expected to be transparent to ballistic phonons, because the interface thickness is of order the wavelength of the athermal phonons. Because we see no difference in the pulses from heater and photon events, our NTD thermistors are likely not very sensitive to the athermal component of the phonons produced in the photon interaction.

3. THE IONIZATION MEASUREMENT

In coincidence with the phonon signal, we also measure the amount of ionization produced by particle interactions in our detector. Our ionization measurement differs from conventional ionization measurements in a few ways. First we use very low drift fields, typically below 1 V/cm. A significantly larger drift field would make discrimination of nuclear recoil events from electron recoil events difficult, because the energy that the charges gain in traversing the detector contributes directly to the total heat measured in phonons. Another difference from conventional ionization detectors operated at warmer temperatures is that our detectors have no thermally excited charge carriers, since $kT \approx 2$ μeV at our operating temperature of ≈ 20 mK. Because of this, free charges present in the crystal during cool down are "frozen out" leaving the crystal initially with a large number of ionized acceptor and donor impurity sites. These ionized sites are very effective traps of the charge

carriers produced by events in the detector, leading to poor charge collection immediately after cool down. To remedy this, the crystal is neutralized by creating a large number of free charge carriers in the detector, either by irradiating the crystal with a strong source of gamma rays, or by illuminating the crystal with an infra-red LED. The charge carriers trap on the impurity sites and neutralize the traps. Once neutralized, the crystal is ready to be used as an ionization detector. However, even after neutralization, the pulse height spectra produced in the detector degrades on the time scale of a few hours; peaks broaden and develop low energy tails. This degradation is believed to be due to a gradual build up of space charge in the detector. The effects due to built-up space charge can be minimized by periodically "resetting" the crystal.[14]

3.1 Charge trapping at the detector edges

Our first detector, E2, had two serious problems in the ionization measurement. A significant number of photon events had much less charge collected than would be expected from the ionization efficiency. The detector also had poor charge resolution of non-penetrating x-ray events. We believe this second problem is due to a dead layer at the ionization collection contacts. The penetrating events with lost charge are believed to be due to charge trapping on the edges of the crystal. The drift field will not be uniform near the edge of the detector because of the disk geometry of E2 and because of static charge buildup on the sides of the detector. Because charge carriers will follow the field lines, charge carriers near the edge of the crystal will trap on the side of the detector. This was confirmed in a series of experiments performed with another detector, E3, described in Young, et al.[15] Two concentric guard rings were added to the ionization contacts so that we could tag events happening near the detector edge. By cutting these events from the data set, most of those with poor charge collection were eliminated.

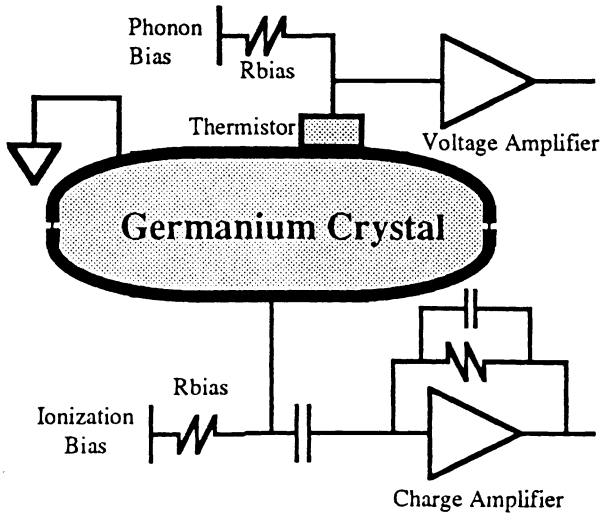

Figure 5. Detector configuration of E4 for the simultaneous detection of phonons and ionization.

To eliminate trapping at the edge of the detector, we rounded the corners and implanted ionization collection contacts over nearly the entire surface; the contact is broken only at a small gap around the equator. (Figure 5) This accomplishes the same task of eliminating poor charge collection that the guard ring did without additional signal channels or significantly reducing the effective volume of the detector. E4 has been tested and has demonstrated essentially the same ionization performance as E3.

4. BACKGROUND REJECTION

A large source of background events in dark matter searches come from low energy photons, which deposit energy in the detector through electron recoils. WIMPs will deposit energy through nuclear recoils. Electron recoils produce proportionately more ionization than nuclear recoils. By examining the ratio of the energy deposited in each channel we can distinguish between nuclear recoils and electron recoils. With our first detector, E2, we demonstrated a background rejection factor of 0.01 for events at 60 keV, and 0.1 for events from 8 keV to 55 keV. [16] Figure 6 shows results from E4. Both plots are histograms of the number of events vs. the ratio of the energy measured in ionization to the energy measured in phonons, for events above 20 keV in phonons. The energy in ionization has been normalized such that $E_Q/E_\phi = 1$ for photons. Figure 6a is with the detector exposed to a ^{241}Am source (photons) and a ^{252}Cf source (neutrons and photons). The gamma events are clearly separated from the neutron events. Figure 6b is with the detector exposed only to the ^{241}Am source. By defining a nuclear recoil window and comparing the two plots, we compute a background rejection factor of 0.008 for events above 20 keV in phonons, and 2 keV in ionization. If we remove the cut on phonons, we find a background rejection factor of .015 for events above 2 keV in ionization. The 18 keV and 14 keV lines from the ^{241}Am source were not clearly resolved because of the dead layer at the ionization contacts. Work is in progress to improve the ionization collection contacts, which may improve the rejection factor at low energies.

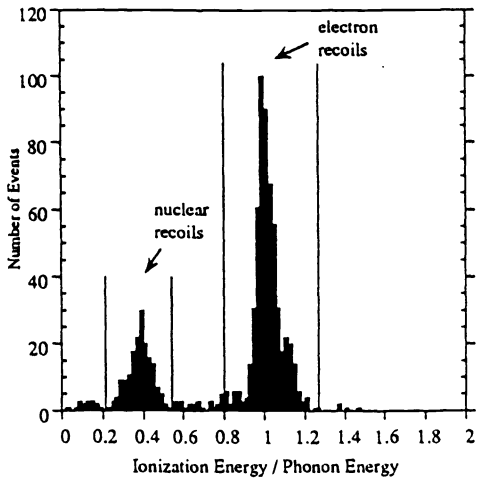

Figure 6a. A histogram of events vs. EQ/ Eφ for E4 with neutrons and gammas. The two types of event are clearly separated.

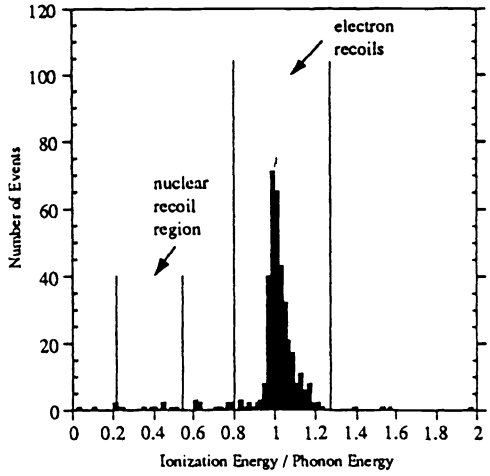

Figure 6b. A histogram of events vs. EQ/ Eφ for E4 with photon source only.

5. ACKNOWLEDGMENTS

This work was supported by the Center for Particle Astrophysics, a National Science Foundation Science and Technology Center operated by the University of California, Berkeley, under Cooperative Agreement No. ADT-8809616, and by the Department of Energy under contract DE-76SF00098.

6. REFERENCES

1. Kolb, E.W. and M.S. Turner, *The Early Universe.* , Addison-Wesley, Redwood City, California, 1990.
2. Alcock, C., *et al.*, "Possible Gravitational Microlensing of a Star in the Large Magellanic Cloud", *Nature*, 365(6447): p. 621-3,1993.
3. Aubourg, E., *et al.*, "Evidence for Gravitational Microlensing by Dark Objects in the Galactic Halo", *Nature*, 365(6447): p. 623-5,1993.
4. Udalski, A., *et al.*, "The Optical Gravitational Lensing Experiment: the discovery of three further microlensing events in the direction of the galactic bulge.", *Astrophysical Journal Letters*, 426(No. 2, Pt. 2): p. L69-72,1994.
5. Primack, J.R., D. Seckel, and B. Sadoulet, "Detection of Cosmic Dark Matter", *Annual Review of Nuclear and Particle Science*, 38: p. 751-807,1988.
6. Stockwell, W., *et al.*, "Low Noise Front End Electronics for Dilution Refrigerator Experiments" in *Fifth International Workshop on Low Temperature Detectors,* Berkeley, 1993. Journal of Low Temperature Physics, Vol. 93, No. 3/4, p. 755-760.
7. Wang, N., *et al.*, "Electrical and Thermal Properties of Neutron Transmutation Doped Germanium at 20 mK.", *Physical Review B*, 41: p. 3761,1990.
8. Aubourg, É., *et al.*, "Measurement of Electron-Phonon Decoupling Time in Neutron-Transmutation Doped Germanium at 20 mK" in *Fifth International Workshop on Low Temperature Detectors*, Berkeley, 1993. Journal of Low Temperature Physics, Vol. 93, No. 3/4, p. 289-294.
9. Knowlton, W.B., *et al.*, "Ge-Au Eutectic Bonding of Ge {100} Single Crystals" in *Fifth International Workshop on Low Temperature Detectors*, Berkeley, 1993. Journal of Low Temperature Physics, Vol. 93, No. 3/4, p. 343-348.
10. Cabrera, B., *et al.*, "Prompt Phonon Signals from Particle Interactions in Si Crystals" in *Fifth International Workshop on Low Temperature Detectors*, Berkeley, 1993. Journal of Low Temperature Physics, Vol. 93, No. 3/4, p. 365-376.
11. Espiov, S.E., *et al.*, "Ballistic Phonon Emission from Electron-Hole Droplets: Application to the Nuclear Recoil Problem" in *Fifth International Workshop on Low Temperature Detectors*, Berkeley, 1993. Journal of Low Temperature Physics, Vol. 93, No. 3/4, p. 377-386.
12. Maris, H. J., "Phonon Physics and Low Temperature Detectors of Dark Matter" in *Fifth International Workshop on Low Temperature Detectors*, Berkeley, 1993. Journal of Low Temperature Physics, Vol. 93, No. 3/4, p. 355-364.

13. Shutt, T., *et al.*, "Simultaneous High Resolution Measurement of Phonons and Ionization Created by Particle Interactions in a 60g Germanium Crystal at 25mK", *Physical Review Letters*, 69: p. 3531,1992.
14. Young, B.A., *et al.*, "A Study of Incomplete Charge Collection in Cryogenic Detectors Using a Segmented 60 gram Germanium Phonon and Ionization Detector" in *Fifth International Workshop on Low Temperature Detectors*, Berkeley, 1993. Journal of Low Temperature Physics, Vol. 93, No. 3/4, p. 393-398.
15. Shutt, T., *et al.*, "Measurement of Ionization and Phonon Production by Nuclear Recoils in a 60g Crystal of Germanium at 25mK", *Physical Review Letters*, 69: p. 3452,1992.